Optics and Lasers in Engineering 165 (2023) 107565

Contents lists available at ScienceDirect

Optics and Lasers in Engineering

journal homepage: www.elsevier.com/locate/optlaseng

Dual-wavelength real-time simultaneous phase imaging based on off-axis interferometry

Xiang Li[a], Guanyuan Qin[a], Yanhua Zou[a], Wenhui Yu[a], Rui Hu[a], Junle Qu[a], Changrui Liao[a,b], Jun He[a,b], Yiping Wang[a,b], Liwei Liu[a,*]

[a] Key Laboratory of Optoelectronic Devices and Systems of Guangdong Province and Ministry of Education, College of Physics and Optoelectronic Engineering, Shenzhen University

[b] Shenzhen Key Laboratory of Photonic Devices and Sensing Systems for Internet of Things, Guangdong and Hong Kong Joint Research Centre for Optical Fiber Sensors, Shenzhen University, Shenzhen 518060, China

ARTICLE INFO

Keywords:
Dual-wavelength
Phase imaging
Off-axis interferometry

ABSTRACT

Dual-wavelength interferometry is widely used in optical measurement, including the of great significance phase imaging of transparent samples. Here, we present a dual wavelength real-time phase imaging system based on off-axis interferometry with two cameras for recording complex fields transmitted through transparent samples in a wide-field and non-intrusive manner. The method of phase unwrapping based on combing dual wavelength with Fourier transform was derived in detail. The advantage of the proposed system is, compared with single-shot dual wavelength holograms methods, that it can easily extract the complex fields at both wavelengths without consideration of spectrum overlap or needing extra optic device to create lateral shearing. For phase noise, we calculated and removed the phase signal without sample in Fourier domain, which can also ensure the measured phase accurately. Experimental results on standard sample (polystyrene microspheres) demonstrated the efficiency of this imaging system. Implementation in quantitative imaging of living cells showed the time of single-shot acquisition of samples was only 0.025s, which indicated that the system can be applied to real-time and label-free identification of phase objects.

1. Introduction

Digital holography (DH) is a well-established technique for optical imaging and tomography measurements [1]. By replacing the photochemical procedures of traditional holography with an electronic imaging sensor, this technique enables the numerical reconstruction and processing of both discrete data and digital images using a computer [2]. In recent decades, thanks to its fast reconstruction speed, high axial resolution, and low cost, DH has been widely used in quantitative phase imaging [3,4].

In conventional DH microscopy, the holograms of target objects are recorded with a single wavelength, which is especially effective for objects with induced optical path delay (OPD) of less than one wavelength. However, ambiguities exist in their reconstructed phase maps which is called phase wrapping. To address this problem, phase unwrapping algorithms can be used by evaluating fringe orders of the wrapped phase map [5]. However, these algorithms are usually computationally slow. Moreover, they cannot correctly unwrap the phase maps when the actual phase differences between two adjacent pixels is greater than 2π. To overcome these problems, dual-wavelength digital holographic techniques (DWDHT) have been proposed [6–16]. In DWDHT, by selecting two appropriate distinct wavelengths, two wrapped phases can be acquired from single-wavelengths holograms. Through direct numerical subtraction of the two wrapped phases, an optical unwrapped phase map of the measured sample at a synthetic wavelength can be achieved. However, the synthetic wavelength, usually in the micron order, is longer than either of the two single wavelengths, which significantly expands the unambiguous phase range. However, previous DWDHT [6,8–12] could not record two holograms simultaneously, limiting their application in dynamic imaging. Although this problem can be resolved by using the four-step phase-shifting method [16], which involves recording four dual-wavelength holograms with a phase shift of $\pi/2$. However, this process is time-consuming and cannot be applied for real-time imaging of living cells or fast-moving objects. Several real-time dual-wavelength digital holographic recording systems have been proposed [17–22,18], wherein it is preferable to record interferograms of two wavelengths simultaneously. In Ref. [17–19], interferograms at two wavelengths were captured in a single shot using a device with a color charge-couple device camera, the limitation of which is that two wavelengths cannot be selected at freely. Therefore, monochrome cameras are more commonly

* Corresponding author.
E-mail address: liulw@szu.edu.cn (L. Liu).

https://doi.org/10.1016/j.optlaseng.2023.107565
Received 18 January 2023; Received in revised form 20 February 2023; Accepted 2 March 2023
Available online 7 March 2023

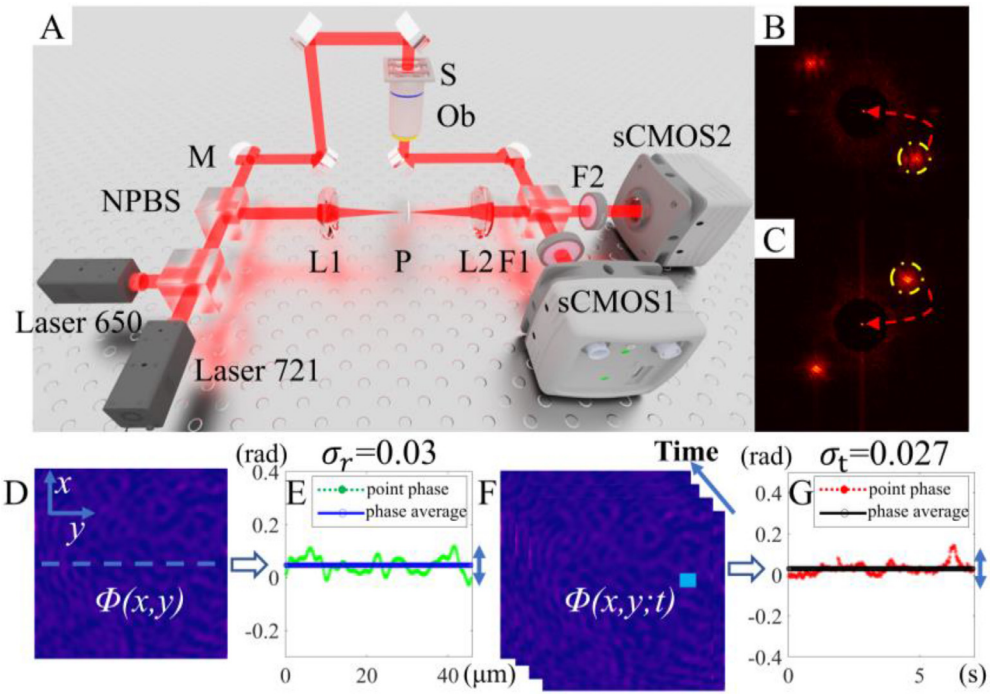

Fig. 1. (A) Experimental system setup. M: mirror; NPBS: non-polarized beam splitter; L1 and L2: Fourier lenses; P: pinhole; S: sample stage; OB: objective lens; F1 and F2: filters of various types; sCMOS: scientific complementary metal-oxide-semiconductor camera; (B) and (C)spatial spectra of the holograms containing the sample at a wavelength of 650 nm and 721 nm, respectively. (D) spatial series of quantitative phase images acquired through the imaging system; (E) phase along the profile shown in (D); (F) time series of quantitative phase images acquired by this imaging system; (G) phase at the blue point shown in (F). σ_r and σ_t: spatial and temporal standard deviation of recorded phase.

used to record multi-wavelength holograms. In [20–22,18], to improve measurement stability and solve frequency-domain overlapping, these systems were employed with extra optical devices, such as a diffractive element [20], grating [21], parallel glass plates [22], dichroic mirrors [18], which resulted in the experiment setup more complex and high cost.

Here, to solve the above problems, we present a dual-wavelength real-time simultaneous phase imaging system based on off-axis interferometry. In this configuration, two types of filters were employed to separate different wavelength beams resulting in two different holograms in separated cameras. Additionally, two identical cameras were inserted in the optical path to receive the processed data. Notably, there was no frequency-domain overlapping to resolve as shown in Fig. 1B-C, when Fourier transform (FT) was used on the holograms. For phase noise, we first acquired the background phase without a sample and then the phase caused only by the sample could be computed by subtracting the background phase. Subsequently, to verify the feasibility of the imaging system, we performed experiments on polystyrene microspheres and living cells, using the concept of phase volume to quantitatively describe the change in the overall sample phase within 2 h, and used the gradient operator to further describe the speed of this change.

2. Materials and methods

2.1. Experimental setup

The experimental setup used for dual-wavelength real-time simultaneous phase imaging based on off-axis interferometry is depicted in Figure 1A. The source comprised two continuous wave (CW) lasers operating at wavelengths of $\lambda 1$ = 650 nm (MRL-III-650L, Changchun New Industry Optoelectronics Technology Co., Ltd., China) and $\lambda 2$ = 721 nm (MRL-III-721L, Changchun New Industry Optoelectronics Technology Co., Ltd., China). The collimated light from the sources was coupled in the first non-polarized beam splitter (NPBS) and then both were separated by the second NPBS into two paths of an imaging Mach-Zehnder interferometer. An objective (GCO-213 40x, Daheng Optics, NA = 0.60) was used to collect and image the sample that was placed on a three-axis displacement table to a scientific complementary metal-oxide-semiconductor (sCMOS) camera (pco.panda.4.2, PCO, Germany). To distinguish the sample beams produced by the two different light sources in parallel, two filters (ET665lp and ET700sp-2p, Chroma Technology Corp, Vermont, U.S.A.) were placed in front of the camera to simultaneously acquire the holograms of different wavelengths. The sCMOS was placed on the imaging plane where an exact (magnified) replica of the sample field could be formed. The acquisition rate of the sCMOS is 40 frames/s at the full resolution of 2048 × 2048 pixels and with pixel size of 6.5 μm. To produce a clean reference beam, spatial filtering was performed using a small pinhole with 30 μm diameter, which was placed within the reference path in the focal plane of the conversion lenses (L1 and L2) with focal length f=125 mm. We used achromatic lenses to minimize chromatic aberration. The reference beams were slightly tilted to the object beam and interfered, forming uniform fringes in sCMOS with an exposure time of 20 ms. Concretely, the typical holograms with dual-wavelength and their Fourier spectrum are shown in Fig. 1B and 1C, with the real and virtual images components for each wavelength interferogram and orthogonal fringe regimes. By selecting the higher-order information in the spectrum to fundamental (as shown by arrows in Fig. 1B and 1C) and performing inverse FT, the wrapped phases directly related to the sample could be obtained. Considering that the absolute value of the phase is not meaningful, the phase recorded by this imaging system has a relative variation induced by the samples and surrounding environment, which means that only one interferogram without samples is initially acquired. However, when the phase distribution is not between $-\pi$ and π, it is necessary to unwrap the true phase resulting from the sample. The true phase signal of the sample can be solved by dual wavelength algorithm based on FT described below. A quantitative way to experimentally assess the phase stability is by performing successive measurements of a stable sample (or no sample). Temporal and spatial sensitivity were used to evaluate the phase measurement accuracy of an imaging system, as shown in Fig. 1(D)-(G), Specifically, the spatial stability of the system could be assessed by measuring the standard deviation of the phase values of 300 pixels in a phase image, as shown in Fig. 1(D)-(E), and the system's time stability was assessed by continuously measuring the standard deviation of the phase values of the same points in 300 phase images, as shown in Fig. 1(F)-(G).

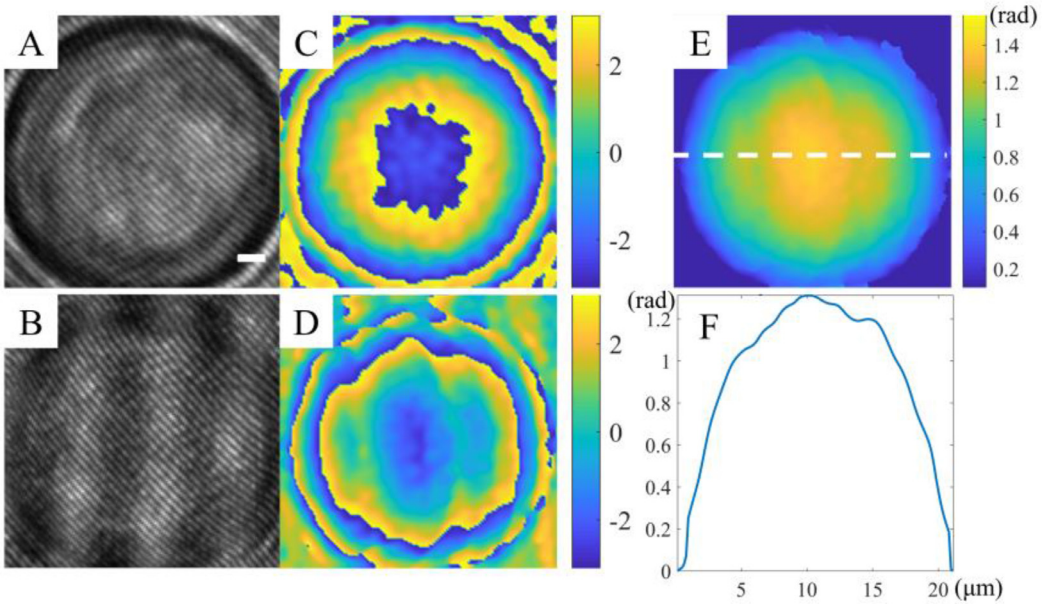

Fig. 2. Phase measurement results of polystyrene microspheres. (A) Hologram image at wavelength of 721 nm; (B) hologram image at wavelength of 650 nm; (C) wrapped phase image at wavelength of 721 nm; (D) wrapped phase image at wavelength of 650 nm; (E) unwrapped phase image at synthetic wavelength; (F) phase profile of horizontal direction curves at the location indicated by the white dashed line shown in (E). Scale bars: 2 μm.

2.2. Dual wavelength based on Fourier Transform (FT)

For the temporal coherence imaging system, by adjusting the angle and intensity between the reference and the object beam, high-contrast holograms can be obtained at the sCMOS. For wavelength $\lambda 1$ ($\lambda 2$ was treated in a similar manner), the holograms with and without samples have following forms respectively:

$$I_{1s} = |U_0|^2 + |U_{1s}|^2 + 2|U_0||U_{1s}|cos(\varphi_1 + \varphi_{sym} + \varphi_n) \tag{1}$$

$$I_0 = |U_0|^2 + |U_1|^2 + 2|U_0||U_1|cos(\varphi_{sym} + \varphi_n) \tag{2}$$

where the $|U_0|^2$ denotes the irradiance distribution of reference, $|U_{1s}|^2$ and $|U_1|^2$are the independent irradiance distribution with and without sample respectively; φ is the optical delay induced by the sample; φ_{sym} is the tilted phase introduced by the reference with respect to the object beam and φ_n is the additional phase modulation provoked by the environment noise. Then, high-frequency information was extracted and returned to the fundamental frequency via the Fourier transform of Eqs. (1) and (2) as shown in Fig. 1B or Fig. 1C. We can get

$$u_{1s}(k_x, k_y)_{\pm 1} = |U_0|\mathcal{F}\left(|U_{1s}(x, y)|e^{\pm j(\varphi_1 + \varphi_n)}\right) \tag{3}$$

$$u_1(k_x, k_y)_{\pm 1} = |U_0|\mathcal{F}\left(|U_1(x, y)|e^{\pm j(\varphi_n)}\right) \tag{4}$$

where $\mathcal{F}$ is the Fourier operator, $u_{1s}(k_x, k_y)$, $u_1(k_x, k_y)$ are the FTs of I_{1s} and I_0 separately. By inverse FTs of $u_{1s}(k_x, k_y)_{\pm 1}$ and $u_1(k_x, k_y)_{\pm 1}$in the spectrum back to the spatial domain, the phase of the sample could be obtained:

$$\varphi_1 = arg\left(\mathcal{F}^{-1}\left(u_{1s}(k_x, k_y)_{+1}\right)./\mathcal{F}^{-1}\left(u_1(k_x, k_y)_{+1}\right)\right) \tag{5}$$

The *arg* represents the two-argument arctangent function atan2 which ranges from -π to π. By dealing with background interference, the influence of coarse fringe is effectively eliminated. Herein, when the thickness of the sample is larger than the wavelength, the phase φ_1 enabled by samples is called wrap phase (φ_2 represented the wrap phase caused by $\lambda 2$). Then, by performing simple mathematical calculations:

$$\phi = \varphi_1 - \varphi_2 = \left(\frac{2\pi}{\lambda_1} - \frac{2\pi}{\lambda_2}\right) \times OPD = 2\pi\frac{OPD}{\Lambda} \tag{6}$$

ϕ is the reconstructed phase for the synthetic beat wavelength and Λ is the synthetic beat wavelength ($\Lambda = \frac{\lambda_1\lambda_2}{\lambda_2 - \lambda_1}$). This beat wavelength is usually tens of times longer than original couple of wavelengths, which enables to resolve much higher structures by removing the phase ambiguity.

3. Results

First, we verified the feasibility and calibrated the system by performing an experiment on a standard sample-polystyrene microsphere which were about 20 μm with refractive index of 1.60. We obtained holograms of the samples at wavelength of 721 nm and 650 nm, as shown in Fig. 2(A) and (B), respectively, in Olympus oil medium with approximate refractive index of 1.52. Fig. 2(C) and (D) show the phase distributions respectively with FT algorithm in a single wavelength. In particular, because the phase of the sample is not distributed in $(-\pi, \pi)$, the FT algorithm cannot compute the solution of the unambiguous phase. By applying above dual-wavelength algorithm, the real synthetic wavelength phase signal was achieved, as shown in Fig. 2(E); the diagram shows the spherical structure of the sample. Additionally, we plotted the phase profile to verify the effectiveness of the proposed imaging system and phase unwrapping method, as shown in Fig. 2(F).

Thereafter, we imaged ovarian carcinoma cells (OCC) of mice. The results of the initial phase recovery of the OCC are shown in Fig. 3. Fig. 3(A)-(B) show hologram images at wavelength of 721 nm and 650 nm, respectively. However, the thickness and refractive index of the cell sample are not large, which still causes the relative phase induced by OCC to produce discontinuities, as shown in Fig. 3(C)-(D). By using the aforementioned method, the synthetic wavelength phase of the cell was obtained, as shown in Fig. 3(E). The phase details shown in Fig. 3(E) were further enhanced through gradient calculation (pointed by arrows in Fig. 3(E) and (F)). Signal to noise ratio and vertical resolution could be also improved by the phase sum [23]. Next, we further processed the synthetic phase of the cells and observed some interesting variation.

To monitor the phase change during natural apoptosis of OCC, we exposed the sample to a culture medium-free environment and observed the morphological changes of ovarian carcinoma over 2 h by measuring the synthetic phase signal of the cells; The results are shown in Fig. 4. It is evident that the structure of the OCC membrane changed significantly,

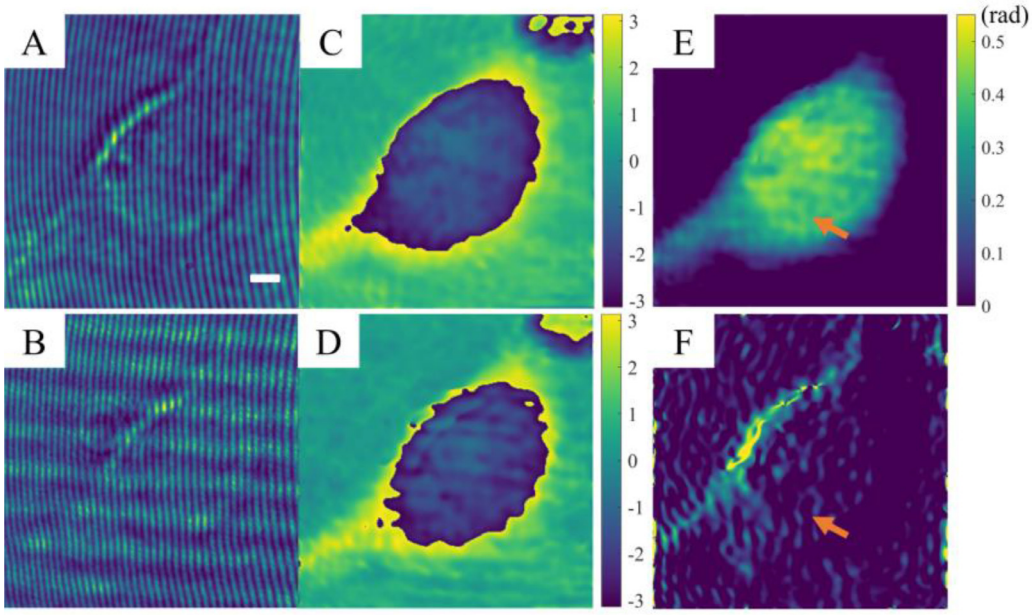

Fig. 3. Phase measurement results of mice OCC. (A) Hologram image at wavelength of 721 nm; (B) hologram image at wavelength of 650 nm; (C) wrapped phase image at wavelength of 721 nm; (D) wrapped phase image at wavelength of 650 nm; (E) unwrapped phase image at synthetic wavelength; (F) gradient transformation of (E) along the horizontal direction. Scale bars: 5 μm.

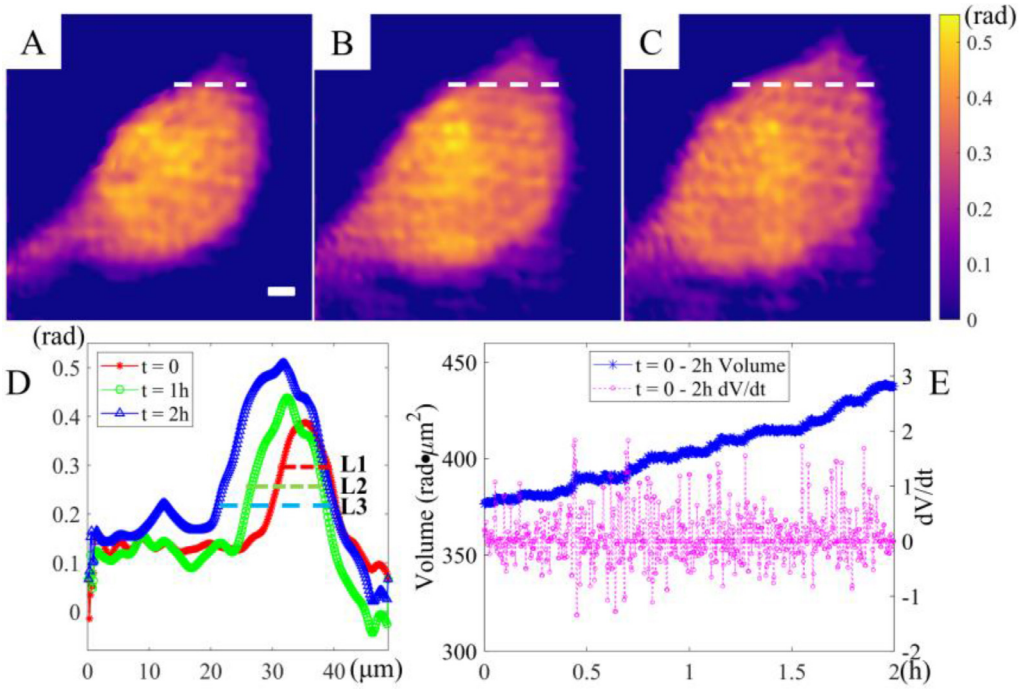

Fig. 4. Results of phase variation tendency measurements in mice OCC. (A) Initial unwrapped phase image at synthetic wavelength; (B) unwrapped phase image at the synthetic wavelength after 1 h; (C) unwrapped phase image at the synthetic wavelength after 2 h; (D) phase profile of horizontal direction curves at the location indicated by the white dashed line shown in (A)–(C). (E) phase volume trend and gradient measurement results of mice OCC. Scale bars: 5 μm.

as shown in Fig. 4(A)-(C). Specifically, the OCC (Fig. 4(A)) has a narrow width along the white dashed line in the phase curve shown in Fig. 4(D). After 1 h, the width along the white dashed line increased, as shown in Fig. 4(B), and it further increased after 2 h, as shown in Fig. 4(C). To quantitatively describe this variation in width of OCC along the white dashed line, we calculated the width values; they were approximately 10 μm (L1), 15 μm (L2), and 20 μm (L3), as shown in Fig. 4(D). The results indicate that the cell membrane morphology changed and apoptosis occurred during the process. To quantitatively show the phase variation of OCC over 2 h, we calculated the synthetic phase volume of the cells at intervals of approximately 10 s. The specific calculation formula is as follows:

$$V_{\varphi} = \iint \varphi(x, y) dx dy \tag{7}$$

Where $\varphi(x, y)$ is the synthetic phase of OCC and dx and dy denote the width and height of each pixel, respectively. The phase volume of OCC

trended to change in one direction nearly and increased constantly, as shown blue line in Fig. 4(E), which indicated that the cell was expanding during apoptosis. Moreover, to quantitatively describe the phase volume variation rate, we calculated the gradient, as shown the purple line in the Fig. 4(E). The gradient value was small in the first 25 min, indicating that the cell changed slowly in the beginning. After that, the gradient value changed dramatically, indicating that the cell's phase volume changed relatively quickly. In general, the phase volume grew at a constant rate over the two hours, but not at an increasing rate all the time, which may be due to the internal structure of the cells and the experimental environment. The dynamic synthetic phase of the OCC was continuously acquired over 2 h at nearly 60 s intervals, as shown in media (See Visualization 1).

4. Discussion and conclusions

We presented a new approach for recording two separated holograms simultaneously to perform phase imaging of transparent objects. For this purpose, digital hologram imaging device based on the Mach Zundel has been extended by using different types of filters to separate the interferograms for the recording process. Then, the acquired hologram could be processed through method reviewed above. The FT algorithm was used owing to its particularly advantageous in frequency-domain spectrum filtering, which can remove the noise and background phase. In the proposed configuration, the time for acquiring single synthetic phase image was approximately 0.025 s with a field of view of 41.6 μm (256 × 256 pixels), which was primarily limited by the exposure time and data transmission rate of the camera. The feasibility of dual wavelength based on FT-based dual-wavelength algorithm was clearly demonstrated through experiments on objects with different phases, such as standard polystyrene microspheres and living biological cell samples. Moreover, we proposed the concept of phase volume, particularly for cell samples, to quantitatively represent the phase information of the entire sample, which can accurately reflect the changes of the sample during the apoptosis process. Consequently, two (sCMOS) cameras based on continuous wave (CW) lasers were introduced in the interferometer setup to capture samples' phase information, the experimental results verified the ability of our system for real-time simultaneous phase measurements. we believe that this work can be helpful to the physiological detection of living cells.

Data availability

The data underlying the results presented in this paper are not publicly available at this time but may be obtained from the authors upon reasonable request.

Funding

We thank the Development Program of China (2021YFF0502900), the National Natural Science Foundation of China (62175163 /62225505/61935012/61835009/62127819), The National Key Research and Shenzhen Key Projects (JCYJ20200109105404067), Shenzhen Talent Innovation Project RCJC20210706091949022, Shenzhen Science and Technology Planning Project (ZDSYS2021 0623092006020) for financial support.

Declaration of Competing Interest

The authors declare no conflicts of interest.

CRediT authorship contribution statement

Xiang Li: Data curation, Software, Formal analysis, Visualization, Writing – original draft, Writing – review & editing. **Guanyuan Qin:** Formal analysis, Supervision, Investigation. **Yanhua Zou:** Validation, Investigation, Data curation. **Wenhui Yu:** Validation, Investigation, Visualization. **Rui Hu:** Validation, Investigation, Visualization. **Junle Qu:** Visualization, Investigation. **Changrui Liao:** Visualization, Investigation. **Jun He:** Visualization, Investigation. **Yiping Wang:** Investigation. **Liwei Liu:** Supervision, Project administration, Writing – review & editing.

Acknowledgement

We thank students Yanhua Zou in the group for providing samples for our imaging system.

Supplementary materials

Supplementary material associated with this article can be found, in the online version, at doi:10.1016/j.optlaseng.2023.107565.

References

[1] Kreis T. Handbook of Holographic Interferometry[M]. 2005.
[2] Kim MK. Principles and techniques of digital holographic microscopy. J Photonics Energy 2009;1(1):8005.
[3] Asundi A. Digital Holography for MEMS and Microsystem Metrology[M]. 2011.
[4] Huang TS. Digital holography. In: Proceedings of the IEEE; 1971.
[5] Ghiglia D C, Pritt MD. Two-Dimensional Phase Unwrapping: Theory, Algorithms, and Software[M]. Wiley; 1998.
[6] Polhemus C. Two-wavelength interferometry. Appl Opt 1973;12(9):2071–4.
[7] Wagner C, Osten W, Seebacher S. Direct shape measurement by digital wavefront reconstruction and multi-wavelength contouring. Opt Eng 2000;39(1):79–85.
[8] Gass J, Dakoff A, Kim M K. Phase imaging without 2π ambiguity by multiwavelength digital holography. Opt Lett 2003;28(13):1141–3.
[9] Abdelsalam D G, Kim D. Two-wavelength in-line phase-shifting interferometry based on polarizing separation for accurate surface profiling. Appl Opt 2011;50(33):6153.
[10] B YFA, A GP, C BMH, A RMG, A WO. Dual-wavelength image-plane digital holography for dynamic measurement - ScienceDirect. Opt Lasers Eng 2009;47(5):552–7.
[11] Warnasooriya, Kim M K. LED-based multi-wavelength phase imaging interference microscopy. Opt Express 2007;15(15):9239–47.
[12] Yokota M, Ishitobi N. Estimation of inner surface profile of a tube by two-wavelength phase-shifting digital holography. Opt Rev 2010;17(3):166–70.
[13] Wang K, Qian K, Di J, Zhao J. Y4-Net: a deep learning solution to one-shot dual-wavelength digital holographic reconstruction. Opt·Lett 2020;45(15).
[14] Liu L, Shan M, Zhong Z, Liu B. Fast reconstruction of two-wavelength off-axis multiplexed holograms using division-multiplexing and critical sampling. Opt Commun 2019;433:297–302.
[15] Shan Mingguang, Liu L, Zhong Z, Liu B, Zhang Y. Improved phase reconstruction using linear programming for dual-wavelength digital holography. Opt Lasers Eng 2019.
[16] Jeon S, Cho J, Jin J N, Park N C, Park Y P. Dual-wavelength digital holography with a single low-coherence light source. Opt Express 2016.
[17] Pascal Picart, Mounier Denis, Desse J Michel. High-resolution digital two-color holographic metrology. Opt Lett 2008.
[18] Turko Nir A, Shaked Natan T. Simultaneous two-wavelength phase unwrapping using an external module for multiplexing off-axis holography. Opt Lett 2017.
[19] Min Junwei, Zhou Meiling, Yuan Xun, Wen Kai, Tong Xianghua, Peng, Yao Baoli. Optical thickness measurement with single-shot dual-wavelength in-line digital holography. Opt Lett 2018.
[20] Monemhaghdoust Z, Montfort Frédéric, Emery Y, Depeursinge C, Moser C. Dual wavelength full field imaging in low coherence digital holographic microscopy. Opt Express 2011;19(24):24005–22.
[21] Jafarfard MR, Moon S, Tayebi B, DY Kim. Dual-wavelength diffraction phase microscopy for simultaneous measurement of refractive index and thickness. Opt Lett 2014;39(10):2908.
[22] Di J, Li Y, Xie M, Zhang J W, Ma C J, Xi T L, Li E P, Zhao J L. Dual-wavelength common-path digital holographic microscopy for quantitative phase imaging based on lateral shearing interferometry. Appl Opt 2016;55(26):7287.
[23] Servin M, Padilla M, Garnica G. Super-sensitive two-wavelength fringe projection profilometry with 2-sensitivities temporal unwrapping. Opt Lasers Eng 2018.